University of Texas Rio Grande Valley

ScholarWorks @ UTRGV

Chemistry Faculty Publications and Presentations

College of Sciences

8-2021

KNN based piezo-triboelectric lead-free hybrid energy films

Abu Masa Abdullah
The University of Texas Rio Grande Valley

Muhtasim Ul Karim Sadaf
The University of Texas Rio Grande Valley

Farzana Tasnim
The University of Texas Rio Grande Valley

Horacio Vasquez
The University of Texas Rio Grande Valley

Karen Lozano
The University of Texas Rio Grande Valley, karen.lozano@utrgv.edu

See next page for additional authors

Follow this and additional works at: https://scholarworks.utrgv.edu/chem_fac

 Part of the Chemistry Commons, and the Power and Energy Commons

Recommended Citation

Abdullah, Abu Musa, Muhtasim Ul Karim Sadaf, Farzana Tasnim, Horacio Vasquez, Karen Lozano, and M. Jasim Uddin. 2021. "KNN based piezo-triboelectric lead-free hybrid energy films." Nano Energy 86 (August): 106133. https://doi.org/10.1016/j.nanoen.2021.106133.

This Article is brought to you for free and open access by the College of Sciences at ScholarWorks @ UTRGV. It has been accepted for inclusion in Chemistry Faculty Publications and Presentations by an authorized administrator of ScholarWorks @ UTRGV. For more information, please contact justin.white@utrgv.edu, william.flores01@utrgv.edu.

Authors

Abu Masa Abdullah, Muhtasim Ul Karim Sadaf, Farzana Tasnim, Horacio Vasquez, Karen Lozano, and M. Jasim Uddin

This article is available at ScholarWorks @ UTRGV: https://scholarworks.utrgv.edu/chem_fac/142

KNN based Piezo-Triboelectric Lead-Free Hybrid Energy Films

Abu Musa Abdullah[1,2], Muhtasim Ul Karim Sadaf[1,3], Farzana Tasnim[1,3], Horacio Vasquez[2], Karen Lozano[2], M Jasim Uddin[1,3,*]

[1] Photonics and Energy Research Laboratory, The University of Texas Rio Grande Valley, 1201 W University Drive, Edinburg, Texas, TX-78539, USA

[2] Department of Mechanical Engineering, The University of Texas Rio Grande Valley, 1201 W University Drive, Edinburg, Texas, TX-78539, USA

[3] Department of Chemistry, The University of Texas Rio Grande Valley, 1201 W University Drive, Edinburg, Texas, TX-78539, USA

*Corresponding Author: M. Jasim Uddin (mohammed.uddin@utrgv.edu)

Journal Pre-proof

Abstract

In recent times, triboelectricity and piezoelectricity have been widely explored to obtain electrical energy from surrounding mechanical input. Scientists are focusing towards developing advanced material composites for utilizing piezoelectricity and triboelectricity for energy harvesting and sensory applications. In this work, potassium sodium niobate (KNN) based energy films (EF) have been developed to utilize mechanical energy while simultaneously taking advantage of triboelectric and piezoelectric mechanisms. The KNN particles were synthesized using a wet ball milling technique and then incorporated into a polyvinylidene difluoride (PVDF) matrix together with multi wall carbon nanotubes (MWCNT). The film was used to develop a piezoelectric nanogenerator (PENG) with copper electrodes. The piezoelectric output of the film was further tested utilizing copper electrodes, at variable tapping frequency (60 BPM to 240 BPM) and pressure (10 to 40 psig) were used when activating the pneumatic piston. The open circuit voltage increased with the increase of both tapping frequency and pressure. The maximum piezoelectric output voltage was observed to be 35.3 V while the maximum current was noted as 15.8 µA. The films also showed unique output signals for different types of deformations performed under hand pressure. The film was further utilized to build a piezo-triboelectric hybrid nanogenerator to check its hybrid performance. The maximum output was observed to be 54.1 V and 29.4 µA. This film was integrated with conventional electronic components (bridge rectifiers, resistors, and capacitors) and tested for its ability to harvest energy. The hybrid nanogenerator can charge a 0.1µF capacitor to 9.4 V in 60s. The optimum

output power for the device was measured to be 0.164 W. The film was further attached with a Kapton film and showed a hybrid output of 113.2 V. This experiment endorsed the potential of the KNN based energy films for multifunctional applications like force, pressure, and motion sensing as well as lead free energy harvesting.

Graphical abstract

Potassium sodium niobate (KNN) was synthesized and incorporated into PVDF along with MWCNT to produce lead-free piezoelectric and piezo-triboelectric hybrid energy films. The high piezoelectric and piezo-tribo hybrid output response showed its potential in biomechanical energy harvesting. Besides, the energy film can be utilized for biomechanical motion and pressure sensing operations.

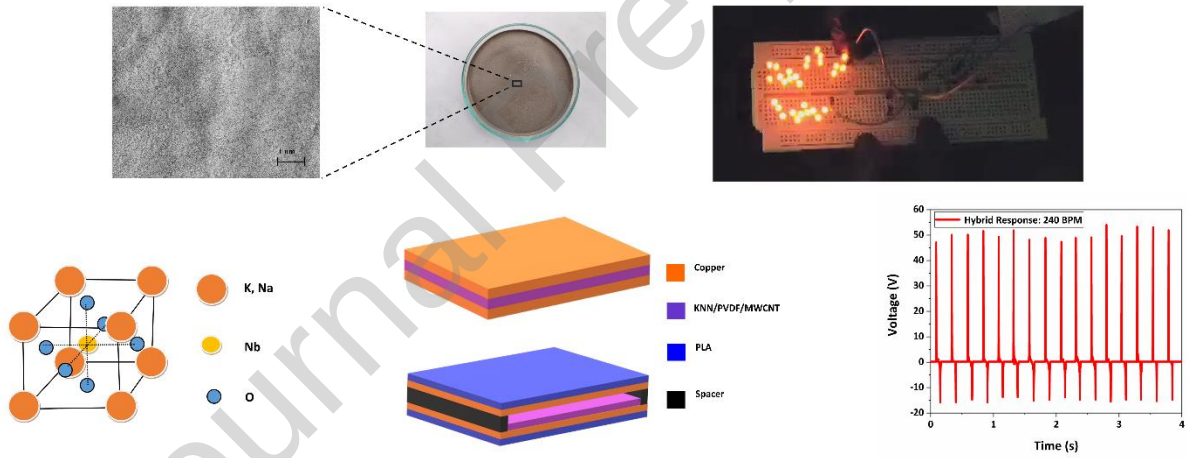

Journal Pre-proof

Keywords

Hybrid Nanogenerator, Piezoelectricity, Triboelectricity, Energy Film, Lead-free Energy Harvesting, Sensor

1. Introduction

Energy deficiency has become a worldwide issue in the twenty-first century [1]. Over the past few decades, intensive efforts have been made to discover alternative energy sources because of the threats represented by the fluctuation of petroleum fuel costs, the danger of climate change, and predicted consumption of non-sustainable fuel sources [2,3]. A potential energy crisis has become the motivation for the fabrication of high-yield materials to scavenge energy from the environment [4].The rapid progress of nanotechnology has received widespread attention by encompassing a continuous study and developing materials with improved properties revealing promising breakthroughs [3]. The piezoelectric effect was discovered by Nobel laureates Pierre and Jacques Curie in 1880 [5]. In 2006, Wang *et al*. [6] made a nanogenerator based on the piezoelectric effect, this was a revolutionary invention moving discoveries closer towards the goal of utilizing and harvesting abundant mechanical energy. Later in 2012, the idea of a nanogenerator utilizing triboelectric phenomena was also introduced by Dr. Wang and his team. The opportunity of using the triboelectric phenomena provides potential for low cost, high power density, lightweight, good flexibility, and highly efficient nanogenerators, they coined the term triboelectric nanogenerator (TENG) [7,8]. Piezoelectric, triboelectric, and a combination of piezoelectric-triboelectric nanogenerators have spearheaded the research in harvesting ambient mechanical energy over the last decade [9,10]. Energy harvesting from human movements have led to a variety of inventions like self-powered devices, sustainable wearable devices, sensors, and actuators [11–14]. Nanogenerators have opened the path towards development of sustainable power sources.

Piezoelectric devices are being used for their thin, flexible, and in some cases, mechanically stretchable structure [5,15], making them suitable for mounting on any type of surface. Developments in materials and manufacturing processes have yielded piezoelectric devices from organic materials that can produce a maximum open-circuit voltage of ~80 V and a short-circuit current of ~300 μA without costly operations such as poling [16]. Triboelectric nanogenerators have also shown superior open-circuit voltage and current. It has been seen that a triboelectric nanogenerator can produce open-circuit voltage of ~4000V with a short-circuit current of ~0.12A [16–18]. Besides, the output power density and energy conversion efficiency of TENG can be as high as 500W/cm^2 and 85% efficiency [19–21]. In a study by Wang *et al.,*

Journal Pre-proof

the performance degradation of TENGs due to natural accumulation of dust and air moisture was studied showing that the upper limit of the performance of TENGs needs to be re-estimated [22]. Another recent study by Lopez *et al.* shows that effective TENGs can be made using commercially available materials and their performance can be increased significantly by simple surface-charge engineering method [23]. Moreover, TENGs have been used for a wide range of applications like wireless energy delivery, self-powered edge ball judgement system in a ping pong game as well as for producing DC current [24–26]. And a recent study by Cao *et al.* showed that all matters when under force, can produce electromagnetic energy which when we combine with triboelectricity, should result in higher outputs [27]. Combination between triboelectric and piezoelectric materials creates hybrid nanogenerators that can produce high and efficient output with a single source of external force [28,29]. In a recent study by Jung *et al.*, a piezoelectric-triboelectric hybrid nanogenerator was constructed and shown to reach an open-circuit voltage of ~370V and a current density of ~12 $\mu A/cm^2$ [16]. Furthermore, these devices are very effective in charging capacitors and very sensitive to forces [4,30], these characteristics show the potential of these devices in sensory applications in addition to harvesting of abundant mechanical energy.

It is very important to choose appropriate materials for the effective utilization of the piezoelectric and triboelectric effect [15,19,31]. Polyvinylidene fluoride (PVDF) is one of the most versatile piezoelectric polymers given its low density, high flexibility, low resistance, and high piezoelectric response [32,33]. PVDF can also work as a tribo-negative polymer [34]. PVDF has several crystalline polymorphs (α, β, γ, δ and ε) depending on the chain conformation [35]. Among all crystalline phases, β and γ are of high priority because of its spontaneous polarization and piezoelectric sensitivity. Several methods are used to induce β phase in PVDF [36]. The stretching, annealing or poling are processes used to transform PVDF from α to β phase [37]. Yu *et al*. [38], and Kim *et al*. [39] confirmed that the use of carbon nanotubes (CNTs) as fillers in a PVDF matrix leads to a relevant increase in the β-phase content. Moreover, multi wall carbon nanotubes (MWCNT) also boost the conductivity of composites by creating a 3D network of conductive MWCNT within the polymer matrix, which ease off electron flow during triboelectric/piezoelectric actions [4]. Kim *et al*. [40] proposed the triboelectric performance of PVDF composites with MWCNTs. Chowdhury *et al*. [4] also demonstrated a

Journal Pre-proof

tribo-piezo hybrid nanogenerator with PVDF/MWCNT/Li-ZnO as the piezoelectric component and PTFE/PDMS as the triboelectric component.

PVDF based composites incorporating various kinds of inorganic materials such as ZnO, $BaTiO_3$(BTO), (K,Na)NbO_3(KNN), $ZnSnO_3$, GaN, and MoS_2 nanoparticles have been explored to fabricate efficient piezoelectric energy harvesters [41]. Lead zirconate titanate (PZT) is also a commonly utilized piezoelectric ceramic material with active materials for mechanical to electrical energy conversions, it has shown higher piezoelectric voltage and dielectric constants than other semiconductor types of piezoelectric materials [42]. Park *et al*. [43], showed a flexible piezoelectric PZT thin film nanogenerator on plastic substrates. Lu *et al*. [44] also discussed multi-material piezoelectric fibers fabricated from perovskite ceramic NPs (BT/PZT)-PVDF and CNT-PVDF composites via fiber drawing. However, due to the high toxicity of PZT, PZT-PVDF fibers are probably not suitable for wearable applications [45]. Nevertheless, the low conductivity of PZT is not ideal for output performance [41]. Synthesizing low-dimensional, single-crystal, lead-free piezoelectric nanomaterials can mitigate these issues [15]. Among the available materials, $ZnSnO_3$, a lead-free multifunctional piezoelectric nanomaterial, has lately attracted considerable interest with promising potential applications in numerous fields [41]. Apart from these, especially, alkaline niobates, based on perovskite-type oxide (K,Na) NbO_3, have also been discussed as promising lead free piezoelectric ceramics [46] [47]. Teka *et at*. [48] portrayed work with potassium sodium niobate, (Na,K)NbO_3 (KNN) as a nano piezoelectric filler, because of its large piezoelectric response, ferroelectric properties, and high curie temperature (>400°C) as well as suitability for low cost and lightweight requirements. KNN is well known as a lead-free energy material which can be used with other functional materials for making piezoelectric composites [49,50]. Moreover, KNN has been reported to achieve a d_{33} coefficient of up to 650 pC/N which is superior when compared to the other lead-free piezoelectric ceramics [51]. However, the performance of KNN based nanogenerators still requires higher output for real life and industrial applications. For instance, Bairagi *et al.*, developed piezoelectric nanogenerator based on KNN, PVDF, and CNT which showed a maximum output of 23.24 V and 18 μA, and when not using CNT, the output voltage was ~ 17.5V and ~ 0.522 μA current [52]. Nevertheless, the triboelectric property of PVDF has not been yet utilized.

Journal Pre-proof

In this work, we have synthesized KNN through ball milling process and incorporated the synthesized KNN into a PVDF matrix along with MWCNT to fabricate lead-free hybrid energy films (EF) for harvesting mechanical energy through triboelectric and piezoelectric mechanisms and we have provided a comprehensive analysis of the piezoelectric and triboelectric properties as well as the potential applications the energy film possesses. The synthesized KNN particles were characterized using X-Ray diffraction (XRD) spectroscopy and scanning electron microscopy (SEM). The film was equipped with copper electrodes to be converted into a PENG and tested at variable load frequencies (60, 120, 180 and 240 BPM). The output piezoelectric voltage of the device was also tested at variable pressures from 10 to 40 PSI utilizing a pneumatic piston. Besides, the energy film was studied during different types of finger movement. A hybrid piezoelectric and triboelectric nanogenerator was fabricated to test the effect of triboelectricity along piezoelectricity. Also, three different types of films with 3%, 4% and 5% KNN were synthesized and tested. Furthermore, the hybrid film was integrated with a bridge rectifier, capacitor, and LEDs to check its compatibility with conventional electronic components. Lastly, the energy film was attached with Kapton to utilize the high triboelectric effect of Kapton along with the piezoelectric effect of the energy film. Overall, the experiment was performed with an aim to develop a lead free triboelectric and piezoelectric composite film for efficient biomechanical energy harvesting and sensory applications with an aim for promoting sustainable future.

Journal Pre-proof

2. Experimental Method

2.1. Synthesis of KNN particles

Potassium carbonate (K_2CO_3), sodium carbonate (Na_2CO_3), and niobium pentoxide (Nb_2O_5) (all from Sigma Aldrich) were selected based on the stoichiometric calculation from the following reaction:

$$K_2CO_3 + Na_2CO_3 + 2Nb_2O_5 \longrightarrow 4(K_{0.5}Na_{0.5})NbO_3 + 2CO_2$$

Before starting the process, the carbonates were dried at 200°C for 2h for their hygroscopic nature. Wet ball milling was performed with ethanol as a solvent and stainless-steel balls with a diameter of 0.25in at 1000 RPM in a vortex mixture for 12h in a sealed round bottom Pyrex glass. After the milling, the mixture was dried at 120°C for 24h. Then, the dried materials were calcined at 900°C for 6h to obtain the KNN particles.

2.2 Preparation of the KNN/PVDF/MWCNT Composite Film

PVDF pellets (Sigma Aldrich) and Multi Walled Carbon Nanotubes (MWCNT) were added in N, N-Dimethylformamide (DMF) (Sigma Aldrich) and the solution was stirred at 400 rpm for 1h at 60°C. Then, the synthesized KNN nanoparticles were added to the DMF solution and placed in a water bath for 30 min at 30°C. After that, the solution was continuously stirred for 24h at 400 rpm and 60°C. The mixture was then cast on the Cu electrode film and dried for 24h at 60^0C to generate the KNN/PVDF/MWCNT composite films.

2.3 Preparation of the Piezoelectric and Piezoelectric-Triboelectric Hybrid Nanogenerator (PTENG)

Copper tape was added on both sides of the synthesized KNN/PVDF/MWCNT composite film to create a piezoelectric nanogenerator. The poling of the piezoelectric film was performed at 80°C for 2h with applied voltage of 4 KV. To create the piezoelectric-triboelectric hybrid nanogenerator (PTENG), polyurethane (PU) spacers were added between the copper tape and the top part of the synthesized composite film. This created an airgap which enabled a triboelectric action parallel to the piezoelectric action. A 2 in^2 polylactic acid (PLA) layer was attached to the outer side of both electrodes to impart rigidity.

Journal Pre-proof

2.4 FTIR Characterization

The Fourier Transform Infrared Spectra of the PVDF film, KNN particles, and the KNN/PVDF/MWCNT composite film were conducted using the VERTEX 70v FTIR Spectrometer (Bruker). The analyzed range was between 450cm^{-1} to 4500cm^{-1} where transmittance was recorded for each sample and the resolution for the analysis was 4 s^{-1}.

2.5 XRD Characterization

The XRD of the KNN was performed using the Rigaku Miniflex X-ray diffractometer. The output data were collected in the 2Θ range from 20° to 60° with a scanning step size of 0.015°.

2.6 SEM characterization

Scanning Electron Microscopy was conducted utilizing a Carl Zeiss Sigma VP Scanning Electron Microscope.

2.7 Output Measurement

The piezoelectric and hybrid output voltage signals were characterized using the Tektronix TDS1001B digital oscilloscope. The signals were further characterized by the VersaSTAT3 potentiostat; this device was used to analyze the potential of the piezoelectric and hybrid film as an energy harvester. This was conducted by connecting the film with bridge rectifiers and capacitors and then analyzing their signals with the potentiostat. The current was measured using a Stanford Research System SR570 current preamplifier.

Journal Pre-proof

3. Result and Discussion

3.1 Characterization of the Synthesized Nanoparticles

Figure 1a shows the XRD pattern of synthesized KNN. Sharp peaks can be observed from the pattern at (100), (110), (002), (200) and (211) from 20° to 60° angle. These peaks clearly denote the formation of the perovskite crystalline structure (Fig 1b) of the KNN particles [53,54]. No impurities can be observed from K, Na or NbO_3. Besides, the sharp peaks of the pattern state the high crystalline quality of the KNN particles.

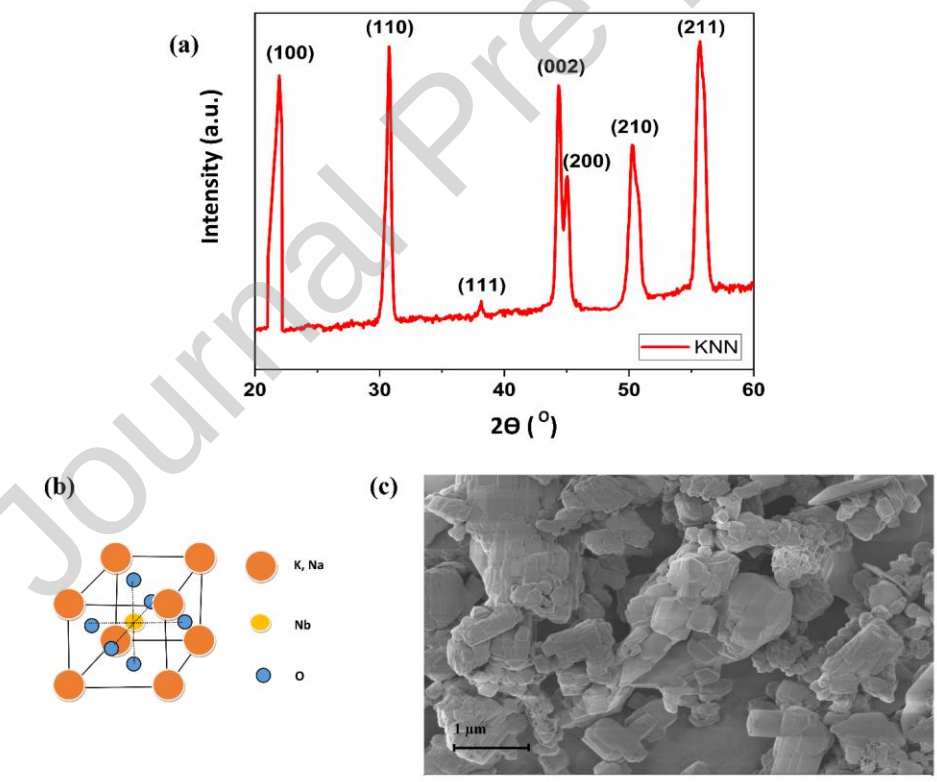

Figure 1: (a) X-ray Diffraction pattern of synthesized KNN powder. (b) Perovskite crystal structure of KNN (c) SEM image of KNN powder

Journal Pre-proof

These results and SEM image indicate that the KNN particles of perovskite structure with orthorhombic phase have been obtained. Diffraction peaks resulting from impurities have been minimized with increasing the calcination temperature to 900° C. The sharp peaks and the peak split around 2θ at 45° are attributed to the purity of the KNN [55]. In addition, no pyrochlore phases are detected. The structures of the KNN particles were further studied using SEM. Fig 1c shows the SEM image of the synthesized KNN particles with a 1μm scale. The dimension of these synthesized cubic particles varied from 80 nm to 300 nm. The SEM also confirms the high degree in grain uniformity and morphology compared to the KNN nanoparticles produced at lower calcination temperatures [56]. Lower particle size could have been achieved by reducing the calcination temperature but that would have been achieved at the cost of losing grain uniformity and morphology [55].

3.2 Characterization of the KNN/PVDF/MWCNT Based Triboelectric and Piezoelectric Energy Film

Journal Pre-proof

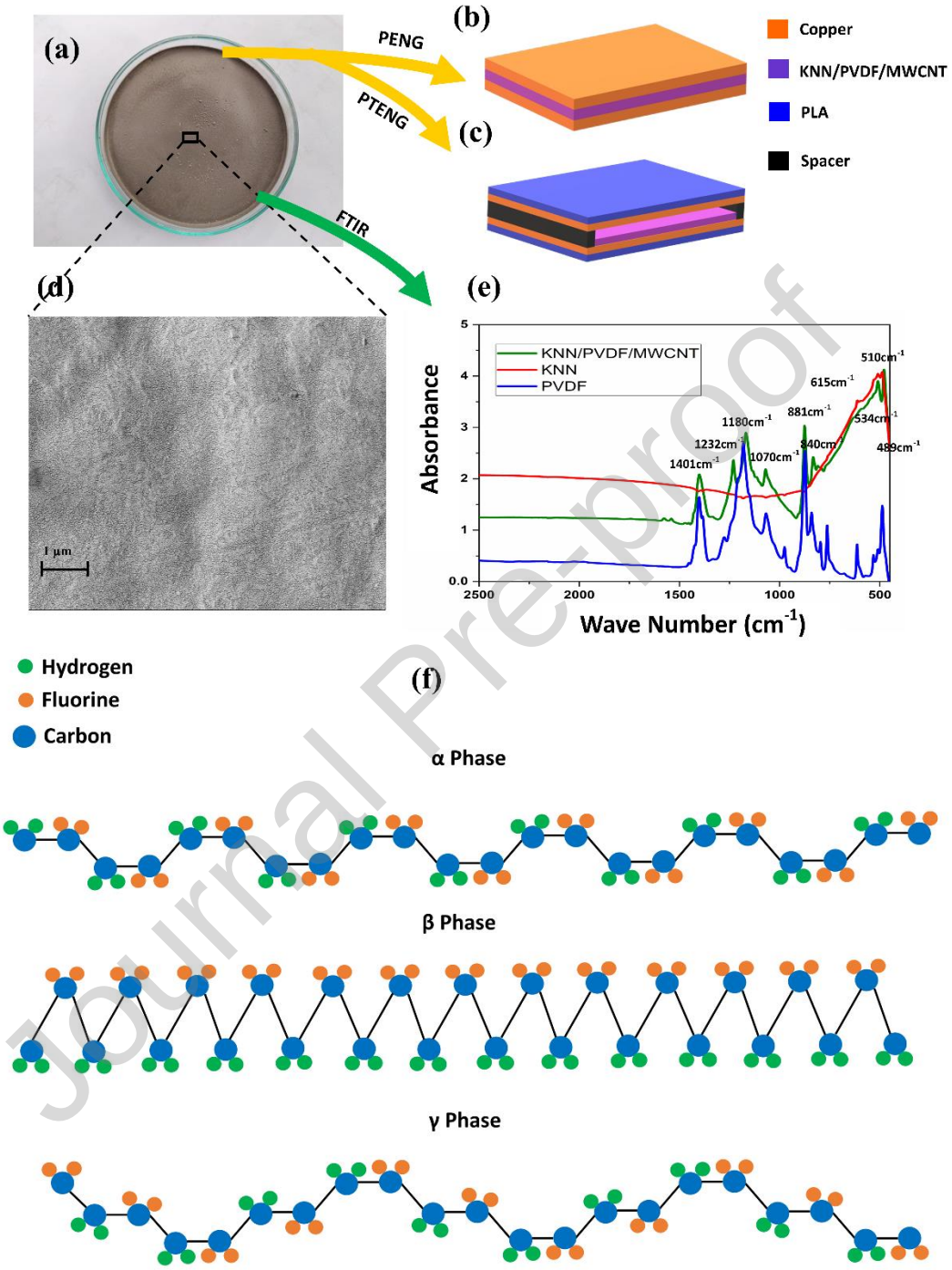

Journal Pre-proof

Figure 2: (a) Optical view of the synthesized KNN/PVDF/MWCNT film. Implementation of the energy film as (b) a PENG and as (c) Hybrid PTENG. (d) SEM image of the surface of the energy film (e) FTIR spectroscopy of the energy film (f) α, β and γ crystalline phases of PVDF

Figure 2a shows the optical image of the film composed of PVDF, KNN, and MWCNT. The EF can be used as PENG by attaching electrodes in both sides. The sandwiched EF along with the electrodes are shown in figure 2b. Copper has been used for the electrodes given its excellent conductivity and availability [57,58]. Additionally, a PTENG was synthesized with the EF (Figure 2c) by attaching the Cu electrode with upper side of the film and attaching the other Cu electrode with a polyurethane (PU) spacer of 1cm in thickness. The whole PTENG structure was reinforced with PLA layers added on top of the electrodes on both sides.

SEM studies depict the surface morphology of the EF, Figure 2d shows the uniformity of the film; it can be clearly seen that the KNN and MWCNT has dispersed throughout the PVDF film making it uniform. Also, KNN particles were not observed on the surface of the film therefore confirming insertion of the KNN particles within the PVDF polymer matrix.

Figure 2e shows the FTIR spectra for the pure PVDF film, the KNN nanoparticles, and the PVDF/KNN/MWCNT composite film. The sharp peaks observed at 881cm^{-1} and 1401cm^{-1} are due to the vibration of C-F stretching and C-H bending of PVDF [59,60]. The peaks around 1180 cm^{-1} of the PVDF in the EF film indicates the presence of both β and γ crystalline phases at high intensity [61]. Besides, the peaks at 510 cm^{-1}, 840 cm^{-1} and 1070 cm^{-1} strongly correspond to the presence of β phase [37,60,62]. Peaks observed at 1232 cm^{-1} and 489 cm^{-1} correspond to the γ phase development [61,63]. It seems from the FTIR spectra that the sample is dominant on β phase with some presence of γ phase. The presence of β phase in the film is very significant for the piezoelectric effect [37]. The γ phase provides some stability to the film as γ phase is more stable at higher temperature enabling the γ phase to stem the diminution of polarization over time [63,64]. The orientation in α, β and γ crystalline phases of PVDF are

Journal Pre-proof

demonstrated in figure 2f. For the KNN, we see an emergence of a broad peak right under the wave number 1000 cm^{-1}; peaks on that region are characteristic vibrations of the Nb-O octahedron which indicates the formation of a perovskite structure [65–68].

3.3 Piezoelectric Performance of the EF

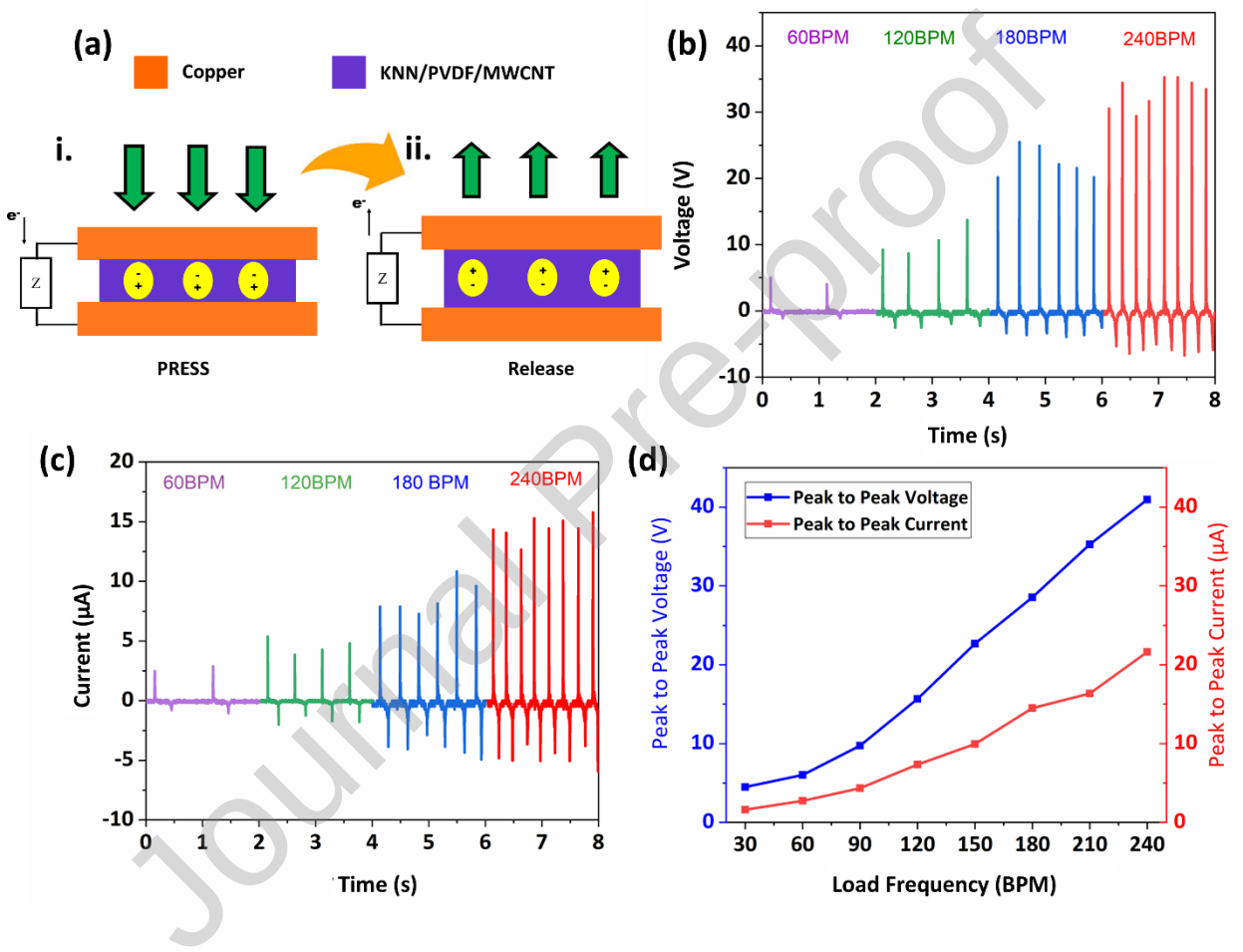

Figure 3: (a) Mechanism of the EF attached PENG: i. Press stage ii. Release Stage (b) Output Voltage and (c) Current observed by tapping the EF attached PENG at 60 BPM, 120 BPM, 180 BPM and 240 BPM load frequency (d) Maximum peak to peak voltage and current observed for tapping the EF attached PENG at variable load frequencies.

The piezoelectric response of the EF was measured by applying an external load on the EF attached PENG. Figure 3a demonstrates the working mechanism of the EF attached PENG

Journal Pre-proof

under external pressure. When external vertical force is applied (Figure 3a-i), the crystal structure of KNN and PVDF gets interrupted. It results in orientation of an electric dipole within the crystal structure. This orientation occurs in a direction which is known as stress induced poling effect [69,70]. An overall voltage difference emerges between two electrodes due to this orientation of dipoles. Positive voltage develops at the upper electrode due to attachment of the electrode with positive portion of the dipole. Electron moves from the upper electrode to the bottom electrode resulting a positive voltage signal in the output [15,49]. When the pressure is released from the PENG, the piezoelectric potential gets removed. As a result, electron moves from the bottom electrode to the upper, resulting a negative signal in the output [69,71]. The intensity of the positive peak was higher compared to the negative peak as the positive peak occurred due to the applied stress from the external source while the negative peak is caused by the resilience of the film by itself [72]. The film is under higher pressure during the external load compared to the self-resilience pressure.

The output performance of the EF attached PENG were tested at tapping frequencies of 60 BPM (1 Hz), 120 BPM (2 Hz), 180 BPM (3 Hz), and 240 BPM (4 Hz) keeping 1 in (2.54 cm) distance between the finger and the upper surface. Tapping acts as an external pressure on the device which results in a voltage and current output. Figure 3b and 3c demonstrates the open circuit voltage and short circuit current obtained from the EF attached PENG at variable load frequencies. Both the voltage and the current increase with increasing frequency. The maximum output voltage and current were observed to be 35.3 V and 15.8 µA for 240 BPM load frequency. Additionally, the maximum voltage for 60 BPM, 120 BPM and 180 BPM was observed to be 5 V, 13.7 V and 25.5 V. On the other hand, the maximum output current was recorded as 2.9 µA, 5.3 µA and 10.8 µA for the respective frequencies. With the increase of the

Journal Pre-proof

load frequency the impact acceleration as well as the force applied on the PENG increases. This results in higher strain in the film which contributes to higher piezoelectric potential [73]. Also, the electrons have less time to neutralize the piezoelectric potential due to the increase of tapping frequency. Therefore, an increase in charge accumulation occurs at the electrodes resulting in higher electron flow and output current [74]. Figure 3d shows the maximum peak to peak output voltage and current by the PENG for a tapping frequency of 30 to 240 BPM. The maximum peak to peak voltage and current was noted to be 40.9 V and 21.6 μA respectively. The output signal increased at a lower rate for first 90 BPM load frequency which increased linearly at a higher rate afterwards. Also, voltage increased at a higher rate compared to the current. This denotes the increasing resistance of the system with increases in load frequencies. Since the resistance of the conductor and electrode is a function of the mechanical dimension, the resistance changes with the external force that increases with loading frequencies [75,76].

The piezoelectric performance of the EF was also measured for various loadings of KNN in the EF. KNN loadings range from 3 to 7 wt. %. The EFs were tapped at 60 BPM load frequency with 1cm gap. Supplementary Figure S2 shows the output voltage of EF with the increase in concentration of KNN. The maximum output voltage increased from 2.3 V to 5.24 V with the increase of KNN from 3 to 5 wt. %. However, the output decreased 3.04 V when KNN concentration increased to 7 wt. %. KNN act as piezoelectric fillers in the film. Increasing the percentage of KNN in the film significantly affects the output. KNN contributes to restrict the nucleation of the β phase of the polymer and increases the chance of creating defects within the PVDF matrix [77]. As a result, the output voltage decreased with the increase of KNN after 5 weight percent.

Journal Pre-proof

3.4 Performance of the EF as a Pressure, Force and Finger Motion Sensor

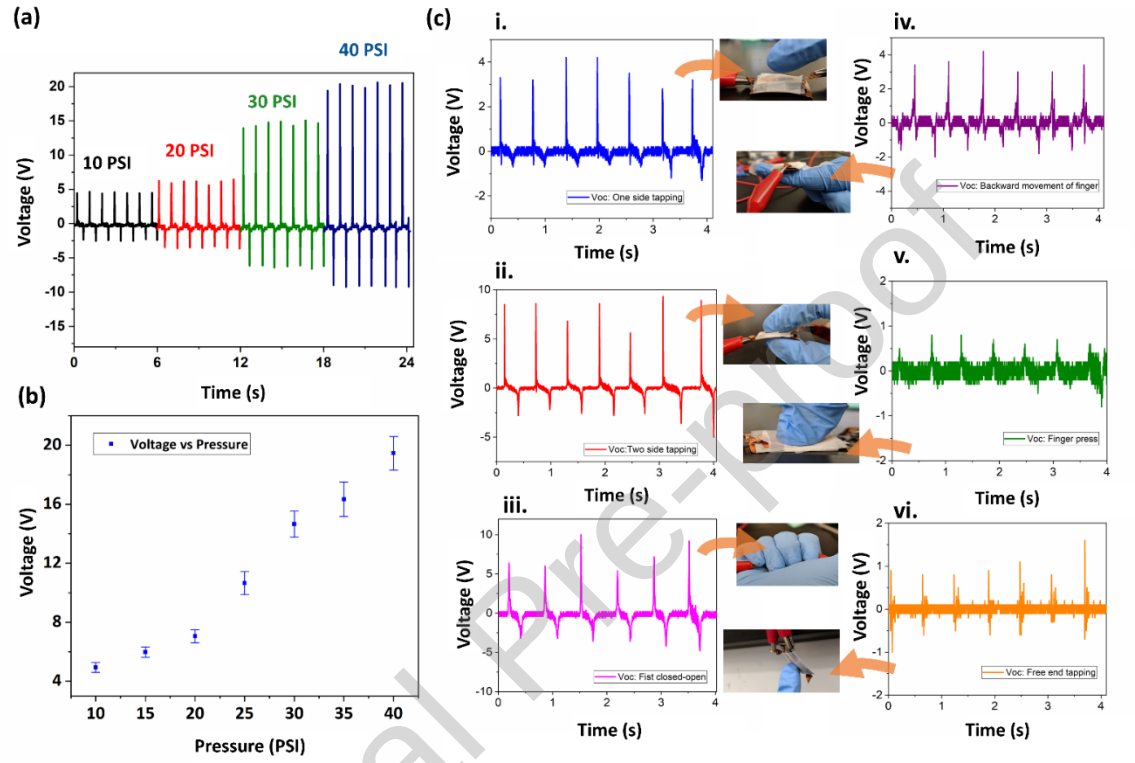

Figure 4: (a) Output piezoelectric voltage signal from the energy film at variable pressure of the pneumatic piston. (b) Maximum voltage observed at variable pressure (Error bars for 95% confidence interval of the mean) (c) Output piezoelectric voltage signal from the energy film for different finger motions: i. One side tapping ii. Two side taping iii. Fist closing and opening iv. Backward movement of finger v. Finger pressing without pulling the finger up vi. Free end tapping.

The response of the EF attached PENG was further tested at variable pressures. The test was performed at 75 BPM loading frequency with a pneumatic piston of 2 cm in diameter. The applied pressure varied from 10 PSI to 40 PSI. The output voltage signals are demonstrated on Figure 4a, this figure clearly shows identical values of the output signal for certain pressure on the device. The maximum output voltage was observed to be 20.6 V for 40 psi. Figure 4b shows the resultant average value of the output voltage by the EF from 10 psi to 40 psi with 5 psi

Journal Pre-proof

interval. The error bars were considered for a 95% confidence interval of the mean. The output voltage clearly increased as a non-linear function of the pressure. With the increase of the pneumatic pressure the force on the EF also increases. The force value can be found by multiplying the pressure with the cross-sectional area of the piston. This increasing force results in the increase of compressive stress on the EF. Consequently, the strain of the EF increases which contributes to the higher piezoelectric voltage in the output. This identical increase of the output voltage with the pressure clearly supports the possible application of the EF as a pressure as well as force sensor.

Figure 4c shows the output signal by the EF under different finger motion. The device was directed towards different finger motions at 120 BPM. The strength and intensity of the touch and the vibration and direction of the motions helps the EF to distinguish between different finger motions [78–81]. This ability promotes its motion sensing operation. Figure 4c-i and 4c-ii demonstrates the output signal for tapping the EF attached from upper and both sides respectively. The maximum output voltage observed for the two-side tapping was 9.3 V while it was 4.4 V for the single side tapping. The output voltage doubled due to the application of force from two sides. Besides, after the application of the stress, the relaxation of the films occurs from both sides. As a result, the negative voltage was observed to be higher and sharper for the two-side tapping. In figure 4c-iii the signal represents the output signal from the EF in closed fist-open fist operation while keeping the device in the fist. The signal is identical with the signal related to two side tapping since the device was directed to force from both sides. The output voltage can be as high as 10 V for this case. Next the PENG was attached to the back of the index finger and the finger was moved backwards freely at 120 BPM frequency in figure 4c-iv. As the finger was attached with the lower electrode of the PENG, force was exerted on the lower

Journal Pre-proof

electrode. This free backward movement resulted in a bending motion of the device. Negative voltage was generated with every free movement of the finger, which however, generates a positive signal whenever the finger moves towards its initial position. The maximum output voltage was observed to be 4.2 V in this test. The signals are observed to be oscillating compared to the double or single side tapping motions. Due to the free end of the motion, additional oscillations can be observed through the signal during every cycle of the free movement [81,82]. The EF was also tested under continuous thumb press at 120 BPM without any distance between the thumb and the device (Fig 4c-v). A single peak can be observed for every press on the PENG. The maximum voltage of this continuous 'w' shaped response was 0.8 V. The zero distance of impact resulted in less force on the PENG which resulted in low output voltage. Figure 4c-vi demonstrates the output response of the EF attached PENG under free end tapping. This can be better defined as a cantilever operation through the PENG. While tapping the film at free end, vibration increases in the film due to the cantilever action mode. This results in additional oscillations in the output response [82,83]. It can be clearly stated from the above discussion that the EF shows identical response and intensity when directed to different finger motions. Therefore, its potential as a sensor to detect biomechanical and finger motions is highly promising. This promotes its implementation as a wearable devices for sensory applications.

3.5. Output performance of EF attached Piezoelectric-Triboelectric Hybrid Nanogenerator

Figures 5a to 5g demonstrate the triboelectric working mechanism of the EF attached PTENG. The triboelectric function of the device occurs due to contact triboelectrification and electrostatic induction [11,19,84]. The initial neutral charge of the device with full airgap is shown in figure 5a. With the application of an external force on the device, the upper layer of Cu moves towards full contact with the EF (Fig 5b). Due to the lower position of PVDF in the

Journal Pre-proof

triboelectric series compared to Cu, electrons transfer to the PVDF surface from the Cu surface which is defined as contact triboelectrification [4,85,86]. The upper electrode moves back to its initial position. The PTENG circle starts operating after the upper electrode of the device starts approaching the EF after contact triboelectrification (Fig 5c). While the upper electrode is moving towards the EF, an electron flow occurs from the upper electrode towards the lower one due to the potential difference between the two electrodes which is the result of electrostatic induction. The upper electrode then comes back to full contact with the EF. The upper electrode is positively charged at this stage to counterbalance the negatively charged EF film. At this stage, the EF goes under full pressure due to the external load (Fig 5d). The piezoelectric dipoles are created at this pressing stage. The electron moves from the upper electrode to the lower electrode due to the piezoelectric voltage. The device shows maximum positive voltage at this position. At the next stage, the external load is withdrawn from the device. As a result, the piezoelectric potential is removed from the device leading towards the flow of the electron from the bottom electrode to the upper electrode. The output voltage starts decreasing. Eventually, the Cu layer starts to move back towards its initial position due to this release of external forces (Fig 5f). To neutralize electrostatic voltage between the two electrodes, electrons from the bottom electrode move towards the positively charged upper electrode. The whole cycle results in alternative current (AC) in the output which continues with the application of the external force. An optical view of the PTENG is demonstrated in Figure 5g.

Journal Pre-proof

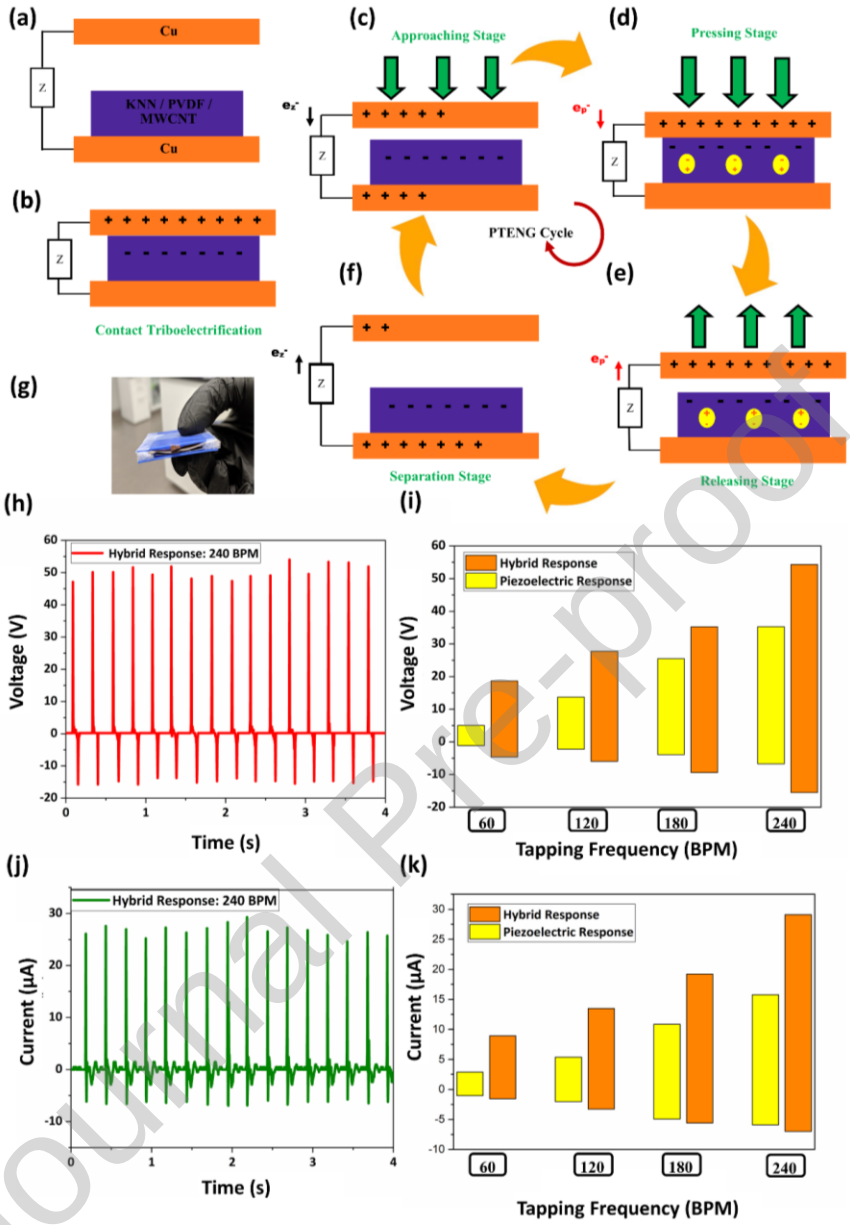

Journal Pre-proof

Figure 5: Working mechanism of the EF attached PTENG (a) EF attached hybrid PTENG at initial stage (b) EF attached PTENG in full contact due to external load (c) Approaching stage: Upper electrode of the EF attached PTENG starts approaching towards the EF due to the repetition of the external force (d) Pressing Stage: EF attached PTENG under fully pressed condition (e) Releasing Stage: Pressure release from the EF attached PTENG due to the removal of external load (f) Separation Stage: Separation of the EF from the upper electrode as the electrode moves towards its initial position (g) Optical view of the EF attached PTENG (h) Output voltage response of the EF attached PTENG at 240 BPM tapping frequency (i) Comparison of the maximum peak to peak voltage between the EF attached PENG and PTENG at 60BPM, 120BPM, 180BPM and 240BPM tapping frequency (j) Output current response of the EF attached PTENG at 240 BPM tapping frequency (k) Comparison of the maximum peak to peak current between the EF attached PENG and PTENG at 60BPM, 120BPM, 180BPM and 240BPM tapping frequency

The hybrid response by the EF attached PTENG at 240 BPM is demonstrated in Figure 5h. The gap between the finger and the device was set to be 1 in. The maximum output and peak to peak voltage of the device was measured to be 54.1 V and 69.4V, respectively. The maximum peak to peak voltage of the hybrid PTENG was compared with maximum peak to peak voltage by the PENG from Figure 5i. The maximum output voltage for the PTENG was 18.6 V, 27.7 V and 35.2 V for the PTENG at 60 BPM, 120 BPM, and 180 BPM load frequencies which came as 5 V, 13.7 V, and 25.5 V for the PENG. The maximum voltage of the PTENG was higher compared to the PENG alone. The combined effect of triboelectricity and piezoelectricity resulted in 18.8 V higher output compared to the piezoelectric voltage alone at 240 BPM. This difference clearly increased with the increasing load frequency. Also, the short circuit current showed a similar trend for the increasing load frequencies. Figure 5j shows the output current by the EF attached PTENG for 240 BPM. The maximum short circuit current was observed to be 29.4 μA. The maximum peak to peak current by the EF attached PTENG was also compared with the output current response by the PENG as shown in Figure 5k. The output current for the PTENG increased from 8.9 μA to 29.1 μA with the increase in frequencies from 60 BPM to 240 BPM. This higher kinetic energy contributes to the flow of electron [19]. Besides, electrons flow at a shorter time to neutralize charge accumulation which results in higher output current [87]. The voltage also increases with the increasing loading frequencies as a linear function of current. [88,89]. The higher triboelectric output with higher frequencies significantly contributes to the output increase for the PTENG at a higher rate compared to the output by the PENG.

Journal Pre-proof

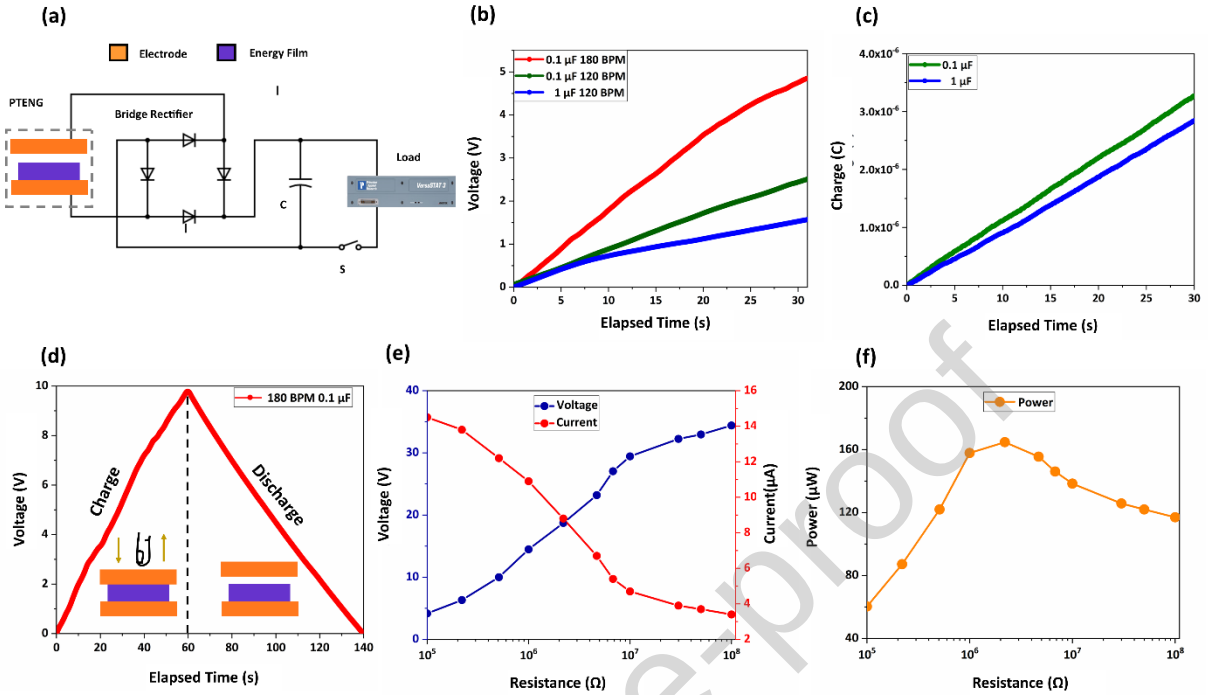

Figure 6: (a) Electrical circuit used for charging the capacitors for EF attached PTENG (b) Charging capacitors for 30s with EF attached PTENG through finger tapping (c) Observed accumulated charge during charging the 0.1 µF and 1 µF capacitors by tapping the EF attached PTENG. (d) Charging and discharging of 0.1 µF capacitors with EF attached PTENG (e) Average voltage and current measured with variable external resistance with EF attached PTENG (f) Average power measured with variable external resistance with EF attached PTENG

The performance of the attached EF was further tested with conventional electronic components. First, it was tested with a full wave bridge rectifier at 120 BPM loading frequency and 1 in finger to top-electrode distance. Supplementary Figure S3 shows the rectified output signal by the PTENG. The signal by the PTENG was completely rectified by the bridge rectifier. Point 1 and 2 indicate the pressing and releasing signals of the EF attached PTENG respectively after the rectifying operation. The maximum voltage after rectifying the voltage was measured to be 18.4 V.

Journal Pre-proof

In another experiment the EF attached PTENG were used as capacitors, its capability to harvest and store energy from mechanical motions and provide constant biased voltage for powering electronic devices was measured [90,91]. The circuitry system used for the test is exhibited in Figure 6a. The device was connected with a full wave bridge rectifier followed by a parallel connection with a capacitor. The VersaStat3 was used in this test. Figure 6b shows the output by the PTENG while charging 0.1 µF and 1 µF capacitors at 120 BPM and 180 BPM for 30s. The maximum voltage after charging the 0.1 µF and 1 µF capacitors at 120 BPM was 2.5 V and 1.6 V respectively. Higher capacitor leads towards higher loss of charges in the capacitor [30,92–94]. Therefore, higher voltage was observed for the 0.1 µF capacitor. Besides, the 0.1 µF capacitor was charged at a higher rate at 180 BPM compared to 120 BPM. The maximum voltage after 30s for 180 BPM loading was observed to be 4.9 V. The larger number of contacts between the surface due to the higher frequency lead towards higher transfer of charges. As a result, higher output voltage as well as higher rate of charging was observed [19,94]. In addition, the accumulated number of charges at the output during the test were observed for the 0.1 µF and 1 µF capacitors (Fig 6c). The charge accumulation in the output increased linearly with time. The number of accumulated charges in the output for the 0.1 µF and 1 µF capacitors at 120 BPM were 3.2 µC and 2.8 µC respectively. The higher loss of charge in the 1 µF capacitor leads toward lower accumulation of charge in the output. Subsequently, the 0.1 µF capacitor was used for a charging-discharging test with the PTENG (Fig 6d). It was frequently tapped for 60s at 180 BPM. The output voltage reached up to 9.8V after 60s (180 cycles). The load was released afterwards. The device took about 80s to discharge. The charging of the device fully depends on the tapping force and frequency, however the discharge of the capacitor occurs at a constant rate

Journal Pre-proof

as there is no external force during discharge [94]. The above results clearly indicate the application of the EF attached PTENG for self-charging operations of electronic devices.

The PTENG was further characterized with external resistance from 10^4 to 10^8 Ω. The output voltage and current for variable external loads is presented in Figure 6e. Following Ohm's law (V=IR) the voltage increases and the current decreases with the increase in resistance. The voltage and current incidents at 2.2 MΩ which can be defined as the optimum point. The power is expected to maximize at this optimum resistance [95,96]. Figure 6f shows the measured output power for variable external load. The maximum power measured was 164.74 μW at 2.2 MΩ (optimum point) external resistance.

3.6: EF and Kapton based PTENG

Journal Pre-proof

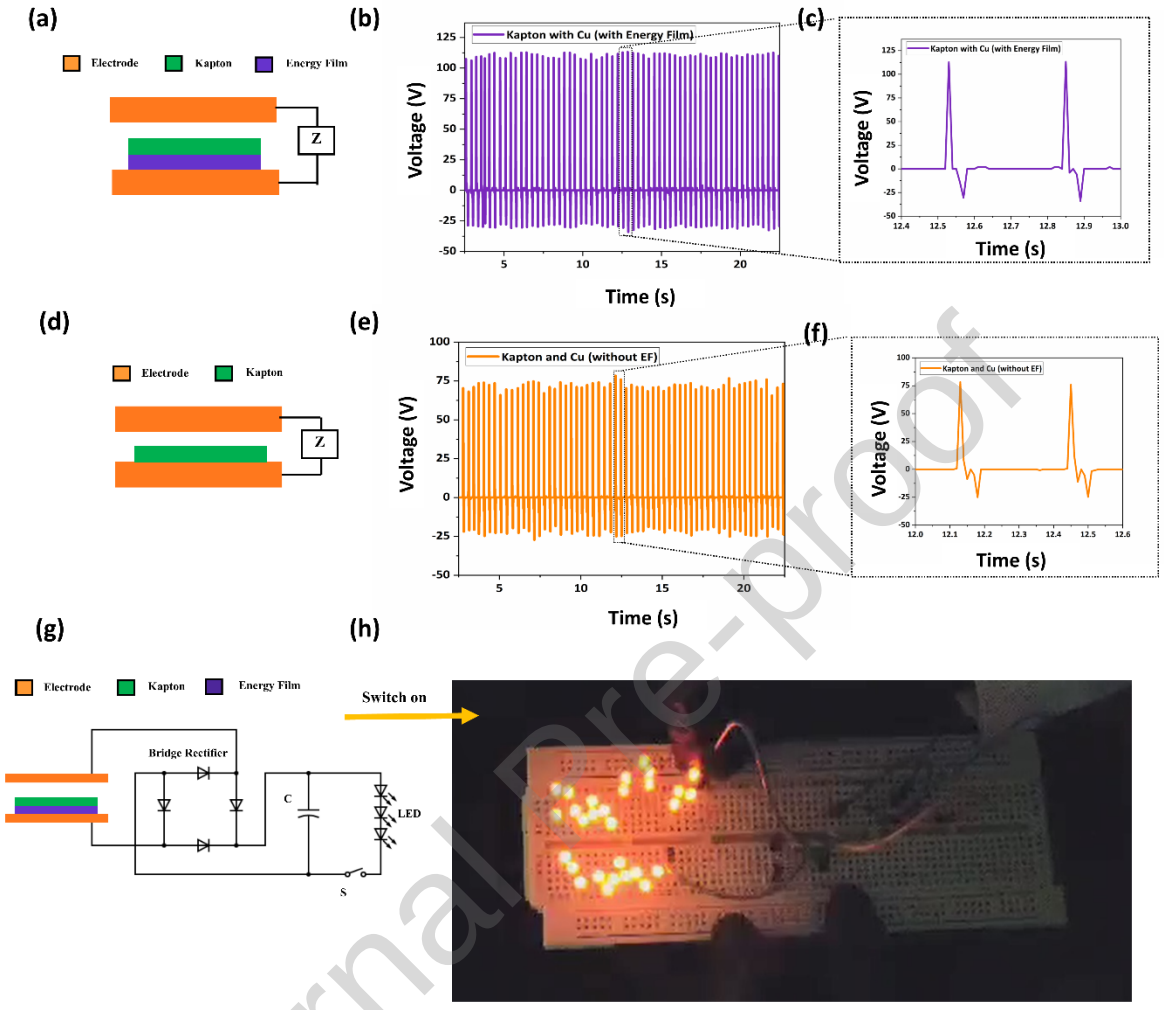

Journal Pre-proof

Figure 7: (a) Schematic of the Nanogenerator with the Cu, Kapton and Energy Film (b) Output voltage of the EF attached Kapton based PTENG at 180 BPM (c) Extended view of the output voltage of the PTENG from 12.4s to 13s (d) Schematic of the Nanogenerator with Cu and Kapton (e) Output voltage of the TENG without EF at 180 BPM (f) Extended view of the output voltage of the PTENG from 12s to 12.6s (g) Electrical circuit used for powering LEDs (h) Lighting LEDs with the EF attached Kapton based PTENG

The EF was further attached with Kapton to fabricate a PTENG for higher output. Kapton is highly known for its triboelectric properties [8,97] The Kapton layer is set over the EF layer along with the Cu electrodes (Fig 7a). The device was tapped at 180 BPM. The output shows a maximum voltage of 113.2 V (Figure 7b). An extended view of the voltage signals is

demonstrated in Figure 7c. A Kapton based Triboelectric Nanogenerator (TENG) was also constructed for comparison purposes (Fig 7d). The Kapton based TENG exhibited a maximum 78.4 V for the same experimental condition. Figure 7e shows the output signal for Kapton based TENG. The extended view of the output signal by the TENG is shown in Figure 7f. It can be clearly stated that the EF is compatible with a Kapton layer to fabricate a PTENG. More importantly, the PTENG shows higher output compared to Kapton based TENG due to the combination of piezoelectricity and triboelectricity from the EF and Kapton respectively.

Durability is an important parameter for a biomechanical energy harvester like PTENG. To test the durability and stability of the device, we performed an experiment on the device for and extended amount of time. When the EF was attached to Kapton, it was subjected to hand tapping at 180 BPM for 3000 cycles where the gap between hand and the PTENG was kept approximately at 1 in. The results are shown in Supplementary Figure S4. No degradation of peaks has been observed throughout the cycle suggesting that the PTENG can take higher loads for an extended amount of time.

The EF/Kapton based PTENG was further tested with light emitting diodes (LED). An equivalent circuitry diagram is shown in Figure 7a. The circuit included a bridge rectifier, capacitors, and a switch. The LEDs were connected in series. The circuit was switched on after tapping the device for 60s at 120 BPM. 30 LEDs were successfully lighted after switching on the circuit. It is evident from the experiment that the EF has a huge prospect to power small electronic devices. Also, the mechanical energy harvesting capability and sensory characteristics of the piezoelectric and triboelectric EF magnifies its application in self-powered sensory devices. Proper application of the EF will promote the goal of lead-free energy harvesting systems leading towards sustainable development.

Journal Pre-proof

Conclusion

In Summary, KNN was synthesized using the ball milling method to fabricate a piezoelectric and triboelectric hybrid energy film along with PVDF and MWCNT. The EF provided a maximum piezoelectric voltage and current of 35.3 V and 15.8 μA respectively. The film was observed to be sensitive for variable pressure and force. Besides, the energy film was sensitive to various modes of finger motion. The results promote the application of this energy film as a pressure, force, and motion sensor. The film also showed higher output voltage with the increase in the percentage of KNN (up to 5% by weight). The film was successfully utilized as piezoelectric/triboelectric hybrid nanogenerator for higher output voltage. The maximum voltage and current during the hybridization were noted as 54.1V and 29.4 μA. The output voltage was observed to be 28.8 V higher compared to the previous studies regarding KNN and PVDF due to the utilization of both triboelectricity and piezoelectricity. Furthermore, the energy film was successfully integrated with bridge rectifiers, capacitors, and LEDs. The energy film showed the capability of charging capacitors of 0.1μF and 1μF. The optimum power for the film was measured to be 164.74 μW with 2.2MΩ load resistance. Additionally, the attachment of Kapton with the energy film showed a high voltage of 113.2 V. 30 LEDs were lighted with this modified device. Overall, this film has a strong potential to develop lead free mechanical energy harvesting devices.

Journal Pre-proof

Reference

[1] I. Hussain, H.P. Tran, J. Jaksik, J. Moore, N. Islam, M.J. Uddin, Functional materials, device architecture, and flexibility of perovskite solar cell, Emergent Mater. 1 (2018) 133–154. https://doi.org/10.1007/s42247-018-0013-1.

[2] F. Tasnim, S.A. Iqbal, A.R. Chowdhury, Biogas production from anaerobic co-digestion of cow manure with kitchen waste and Water Hyacinth, Renewable Energy. 109 (2017) 434–439. https://doi.org/10.1016/j.renene.2017.03.044.

[3] A.M. Abdullah, A.R. Chowdhury, Y. Yang, H. Vasquez, H.J. Moore, J.G. Parsons, K. Lozano, J.J. Gutierrez, K.S. Martirosyan, M.J. Uddin, Tailoring the viscosity of water and ethylene glycol based TiO2 nanofluids, Journal of Molecular Liquids. 297 (2020) 111982. https://doi.org/10.1016/j.molliq.2019.111982.

[4] A.R. Chowdhury, A.M. Abdullah, I. Hussain, J. Lopez, D. Cantu, S.K. Gupta, Y. Mao, S. Danti, M.J. Uddin, Lithium doped zinc oxide based flexible piezoelectric-triboelectric hybrid nanogenerator, Nano Energy. 61 (2019) 327–336. https://doi.org/10.1016/j.nanoen.2019.04.085.

[5] P.K. Panda, Review: environmental friendly lead-free piezoelectric materials, J Mater Sci. 44 (2009) 5049–5062. https://doi.org/10.1007/s10853-009-3643-0.

[6] Z.L. Wang, J. Song, Piezoelectric Nanogenerators Based on Zinc Oxide Nanowire Arrays, Science. 312 (2006) 242–246. https://doi.org/10.1126/science.1124005.

[7] Q. Zheng, B. Shi, Z. Li, Z.L. Wang, Recent Progress on Piezoelectric and Triboelectric Energy Harvesters in Biomedical Systems, Adv Sci (Weinh). 4 (2017) 1700029. https://doi.org/10.1002/advs.201700029.

[8] F.-R. Fan, Z.-Q. Tian, Z. Lin Wang, Flexible triboelectric generator, Nano Energy. 1 (2012) 328–334. https://doi.org/10.1016/j.nanoen.2012.01.004.

[9] B.J. Hansen, Y. Liu, R. Yang, Z.L. Wang, Hybrid Nanogenerator for Concurrently Harvesting Biomechanical and Biochemical Energy, ACS Nano. 4 (2010) 3647–3652. https://doi.org/10.1021/nn100845b.

[10] M. Han, X. Zhang, W. Liu, X. Sun, X. Peng, H. Zhang, Low-frequency wide-band hybrid energy harvester based on piezoelectric and triboelectric mechanism, Sci. China Technol. Sci. 56 (2013) 1835–1841. https://doi.org/10.1007/s11431-013-5270-x.

[11] P. Bai, G. Zhu, Z.-H. Lin, Q. Jing, J. Chen, G. Zhang, J. Ma, Z.L. Wang, Integrated Multilayered Triboelectric Nanogenerator for Harvesting Biomechanical Energy from Human Motions, ACS Nano. 7 (2013) 3713–3719. https://doi.org/10.1021/nn4007708.

[12] A.R. Chowdhury, A.M. Abdullah, U.V. Romero, I. Hussain, C. Olivares, S. Danti, J. Li, M.J. Uddin, Decentralized Triboelectric Electronic Health Monitoring Flexible Microdevice, MEDICAL DEVICES & SENSORS. n/a (2020) e10103. https://doi.org/10.1002/mds3.10103.

[13] L. Jin, J. Tao, R. Bao, L. Sun, C. Pan, Self-powered Real-time Movement Monitoring Sensor Using Triboelectric Nanogenerator Technology, Scientific Reports. 7 (2017) 1–6. https://doi.org/10.1038/s41598-017-10990-y.

[14] Z. Lou, L. Li, L. Wang, G. Shen, Recent Progress of Self-Powered Sensing Systems for Wearable Electronics, Small. 13 (2017) 1701791. https://doi.org/10.1002/smll.201701791.

[15] A.R. Chowdhury, J. Jaksik, I. Hussain, R. Longoria, O. Faruque, F. Cesano, D. Scarano, J. Parsons, M.J. Uddin, Multicomponent nanostructured materials and interfaces for efficient piezoelectricity, Nano-Structures & Nano-Objects. 17 (2019) 148–184. https://doi.org/10.1016/j.nanoso.2018.12.002.

Journal Pre-proof

[16] W.-S. Jung, M.-G. Kang, H.G. Moon, S.-H. Baek, S.-J. Yoon, Z.-L. Wang, S.-W. Kim, C.-Y. Kang, High Output Piezo/Triboelectric Hybrid Generator, Scientific Reports. 5 (2015) 1–6. https://doi.org/10.1038/srep09309.
[17] Y. Xi, J. Wang, Y. Zi, X. Li, C. Han, X. Cao, C. Hu, Z. Wang, High efficient harvesting of underwater ultrasonic wave energy by triboelectric nanogenerator, Nano Energy. 38 (2017) 101–108. https://doi.org/10.1016/j.nanoen.2017.04.053.
[18] F. Liu, Y. Liu, Y. Lu, Z. Wang, Y. Shi, L. Ji, J. Cheng, Electrical analysis of triboelectric nanogenerator for high voltage applications exampled by DBD microplasma, Nano Energy. 56 (2019) 482–493. https://doi.org/10.1016/j.nanoen.2018.11.064.
[19] A.M. Abdullah, A. Flores, A.R. Chowdhury, J. Li, Y. Mao, M.J. Uddin, Synthesis and fabrication of self-sustainable triboelectric energy case for powering smart electronic devices, Nano Energy. 73 (2020) 104774. https://doi.org/10.1016/j.nanoen.2020.104774.
[20] W. Tang, T. Jiang, F.R. Fan, A.F. Yu, C. Zhang, X. Cao, Z.L. Wang, Liquid-Metal Electrode for High-Performance Triboelectric Nanogenerator at an Instantaneous Energy Conversion Efficiency of 70.6%, Advanced Functional Materials. 25 (2015) 3718–3725. https://doi.org/10.1002/adfm.201501331.
[21] Z.L. Wang, Triboelectric nanogenerators as new energy technology and self-powered sensors – Principles, problems and perspectives, Faraday Discuss. 176 (2015) 447–458. https://doi.org/10.1039/C4FD00159A.
[22] J. Wang, C. Wu, Y. Dai, Z. Zhao, A. Wang, T. Zhang, Z.L. Wang, Achieving ultrahigh triboelectric charge density for efficient energy harvesting, Nature Communications. 8 (2017) 88. https://doi.org/10.1038/s41467-017-00131-4.
[23] D. Lopez, A.R. Chowdhury, A.M. Abdullah, M.U.K. Sadaf, I. Martinez, B.D. Choudhury, S. Danti, C.J. Ellison, K. Lozano, M.J. Uddin, Polymer Based Triboelectric Nanogenerator for Cost-Effective Green Energy Generation and Implementation of Surface-Charge Engineering, Energy Technology. n/a (n.d.). https://doi.org/10.1002/ente.202001088.
[24] X. Cao, M. Zhang, J. Huang, T. Jiang, J. Zou, N. Wang, Z.L. Wang, Inductor-Free Wireless Energy Delivery via Maxwell's Displacement Current from an Electrodeless Triboelectric Nanogenerator, Advanced Materials. 30 (2018) 1704077. https://doi.org/10.1002/adma.201704077.
[25] J. Luo, Z. Wang, L. Xu, A.C. Wang, K. Han, T. Jiang, Q. Lai, Y. Bai, W. Tang, F.R. Fan, Z.L. Wang, Flexible and durable wood-based triboelectric nanogenerators for self-powered sensing in athletic big data analytics, Nature Communications. 10 (2019) 5147. https://doi.org/10.1038/s41467-019-13166-6.
[26] J. Luo, L. Xu, W. Tang, T. Jiang, F.R. Fan, Y. Pang, L. Chen, Y. Zhang, Z.L. Wang, Direct-Current Triboelectric Nanogenerator Realized by Air Breakdown Induced Ionized Air Channel, Advanced Energy Materials. 8 (2018) 1800889. https://doi.org/10.1002/aenm.201800889.
[27] X. Cao, Y. Jie, P. Ma, Z.L. Wang, Wherever there is a dynamic touch, there is electromagnetic field——a discovery for power generation, Nano Energy. 78 (2020) 105314. https://doi.org/10.1016/j.nanoen.2020.105314.
[28] H.H. Singh, N. Khare, Flexible ZnO-PVDF/PTFE based piezo-tribo hybrid nanogenerator, Nano Energy. 51 (2018) 216–222. https://doi.org/10.1016/j.nanoen.2018.06.055.
[29] W. Wang, J. Zhang, Y. Zhang, F. Chen, H. Wang, M. Wu, H. Li, Q. Zhu, H. Zheng, R. Zhang, Remarkably enhanced hybrid piezo/triboelectric nanogenerator via rational modulation of piezoelectric and dielectric properties for self-powered electronics, Appl. Phys. Lett. 116 (2020) 023901. https://doi.org/10.1063/1.5134100.
[30] Simiao Niu, Ying Liu, Yu Sheng Zhou, Sihong Wang, Long Lin, Zhong Lin Wang, Optimization of Triboelectric Nanogenerator Charging Systems for Efficient Energy Harvesting and Storage, IEEE Trans. Electron Devices. 62 (2015) 641–647. https://doi.org/10.1109/TED.2014.2377728.

Journal Pre-proof

[31] A.M. Abdullah, A. Flores, A. Chowdhury, J. Li, Y. Mao, M.J. Uddin, Corrigendum to “Synthesis and fabrication of self-sustainable triboelectric energy case for powering smart electronic devices” [Nano Energy, Volume 73, July 2020, 104774], Nano Energy. 76 (2020) 104996. https://doi.org/10.1016/j.nanoen.2020.104996.
[32] H.B. Kang, C.S. Han, J.C. Pyun, W.H. Ryu, C.-Y. Kang, Y.S. Cho, (Na,K)NbO3 nanoparticle-embedded piezoelectric nanofiber composites for flexible nanogenerators, Composites Science & Technology. 111 (2015) 1–8. https://doi.org/10.1016/j.compscitech.2015.02.015.
[33] A.R. Chowdhury, Organic-Inorganic Hybrid Materials for Piezoelectric/Triboelectric Nanogenerator, M.S., The University of Texas Rio Grande Valley, 2020. https://search.proquest.com/docview/2298135475/abstract/8B4E6CC082914532PQ/1 (accessed February 12, 2021).
[34] Q. Jing, S. Kar-Narayan, Nanostructured polymer-based piezoelectric and triboelectric materials and devices for energy harvesting applications, J. Phys. D: Appl. Phys. 51 (2018) 303001. https://doi.org/10.1088/1361-6463/aac827.
[35] Y. Koseki, K. Aimi, S. Ando, Crystalline structure and molecular mobility of PVDF chains in PVDF/PMMA blend films analyzed by solid-state 19 F MAS NMR spectroscopy, Polymer Journal. 44 (2012) 757–763. https://doi.org/10.1038/pj.2012.76.
[36] B. Bera, M. Sarkar, Piezoelectricity in PVDF and PVDF Based Piezoelectric Nanogenerator: A Concept, IOSR Journal of Applied Physics. 09 (2017) 95–99. https://doi.org/10.9790/4861-0903019599.
[37] L. Ruan, X. Yao, Y. Chang, L. Zhou, G. Qin, X. Zhang, Properties and Applications of the β Phase Poly(vinylidene fluoride), Polymers (Basel). 10 (2018). https://doi.org/10.3390/polym10030228.
[38] S. Yu, W. Zheng, W. Yu, Y. Zhang, Q. Jiang, Z. Zhao, Formation Mechanism of β-Phase in PVDF/CNT Composite Prepared by the Sonication Method, Macromolecules. 42 (2009) 8870–8874. https://doi.org/10.1021/ma901765j.
[39] G.H. Kim, S.M. Hong, Y. Seo, Piezoelectric properties of poly(vinylidene fluoride) and carbon nanotube blends: beta-phase development, Phys Chem Chem Phys. 11 (2009) 10506–10512. https://doi.org/10.1039/b912801h.
[40] S. Kim, Y. Song, M.J. Heller, Influence of MWCNTs on β-Phase PVDF and Triboelectric Properties, Journal of Nanomaterials. 2017 (2017) e2697382. https://doi.org/10.1155/2017/2697382.
[41] R. Guo, Y. Guo, H. Duan, H. Li, H. Liu, Synthesis of Orthorhombic Perovskite-Type ZnSnO3 Single-Crystal Nanoplates and Their Application in Energy Harvesting, ACS Appl. Mater. Interfaces. 9 (2017) 8271–8279. https://doi.org/10.1021/acsami.6b16629.
[42] X. Chen, S. Xu, N. Yao, Y. Shi, 1.6 V Nanogenerator for Mechanical Energy Harvesting Using PZT Nanofibers, Nano Lett. 10 (2010) 2133–2137. https://doi.org/10.1021/nl100812k.
[43] K.-I. Park, J.H. Son, G.-T. Hwang, C.K. Jeong, J. Ryu, M. Koo, I. Choi, S.H. Lee, M. Byun, Z.L. Wang, K.J. Lee, Highly-Efficient, Flexible Piezoelectric PZT Thin Film Nanogenerator on Plastic Substrates, Advanced Materials. 26 (2014) 2514–2520. https://doi.org/10.1002/adma.201305659.
[44] X. Lu, H. Qu, M. Skorobogatiy, Piezoelectric Micro- and Nanostructured Fibers Fabricated from Thermoplastic Nanocomposites Using a Fiber Drawing Technique: Comparative Study and Potential Applications, ACS Nano. 11 (2017) 2103–2114. https://doi.org/10.1021/acsnano.6b08290.
[45] X. Lu, H. Qu, M. Skorobogatiy, Piezoelectric Microstructured Fibers via Drawing of Multimaterial Preforms, Scientific Reports. 7 (2017) 1–12. https://doi.org/10.1038/s41598-017-01738-9.
[46] Y. Shiratori, A. Magrez, W. Fischer, C. Pithan, R. Waser, Temperature-induced Phase Transitions in Micro-, Submicro-, and Nanocrystalline NaNbO 3, The Journal of Physical Chemistry C. 111 (n.d.) 18493–18502.

Journal Pre-proof

[47] T.-Y. Ke, H.-A. Chen, H.-S. Sheu, J.-W. Yeh, H.-N. Lin, C.-Y. Lee, H.-T. Chiu, Sodium Niobate Nanowire and Its Piezoelectricity, J. Phys. Chem. C. 112 (2008) 8827–8831. https://doi.org/10.1021/jp711598j.
[48] A. Teka, S. Bairagi, M. Shahadat, M. Joshi, S.Z. Ahammad, S.W. Ali, Poly(vinylidene fluoride) (PVDF)/potassium sodium niobate (KNN)–based nanofibrous web: A unique nanogenerator for renewable energy harvesting and investigating the role of KNN nanostructures, Polymers for Advanced Technologies. 29 (2018) 2537–2544. https://doi.org/10.1002/pat.4365.
[49] S. Bairagi, S.W. Ali, Influence of High Aspect Ratio Lead-Free Piezoelectric Fillers in Designing Flexible Fibrous Nanogenerators: Demonstration of Significant High Output Voltage, Energy Technology. 7 (2019) 1900538. https://doi.org/10.1002/ente.201900538.
[50] S. Bairagi, S.W. Ali, Flexible lead-free PVDF/SM-KNN electrospun nanocomposite based piezoelectric materials: Significant enhancement of energy harvesting efficiency of the nanogenerator, Energy. 198 (2020) 117385. https://doi.org/10.1016/j.energy.2020.117385.
[51] X. Lv, J. Zhu, D. Xiao, X. Zhang, J. Wu, Emerging new phase boundary in potassium sodium-niobate based ceramics, Chem. Soc. Rev. 49 (2020) 671–707. https://doi.org/10.1039/C9CS00432G.
[52] S. Bairagi, S.W. Ali, Investigating the role of carbon nanotubes (CNTs) in the piezoelectric performance of a PVDF/KNN-based electrospun nanogenerator, Soft Matter. 16 (2020) 4876–4886. https://doi.org/10.1039/D0SM00438C.
[53] J. Hao, Z. Xu, R. Chu, Y. Zhang, Q. Chen, P. Fu, W. Li, G. Li, Q. Yin, Characterization of (K0.5Na0.5)NbO3 powders and ceramics prepared by a novel hybrid method of sol–gel and ultrasonic atomization, Materials & Design. 31 (2010) 3146–3150. https://doi.org/10.1016/j.matdes.2009.12.015.
[54] Q. Chai, X. Zhao, X. Chao, Z. Yang, Enhanced transmittance and piezoelectricity of transparent $K_{0.5}Na_{0.5}NbO_3$ ceramics with $Ca(Zn_{1/3}Nb_{2/3})O_3$ additives, RSC Adv. 7 (2017) 28428–28437. https://doi.org/10.1039/C7RA04064D.
[55] Gh.H. Khorrami, A. Kompany, A. Khorsand Zak, A facile sol–gel approach to synthesize KNN nanoparticles at low temperature, Materials Letters. 110 (2013) 172–175. https://doi.org/10.1016/j.matlet.2013.07.115.
[56] Y. Zhao, Y. Chen, K. Chen, Improvement in synthesis of (K0.5Na0.5)NbO3 powders by Ge4+ acceptor doping, Front. Mater. Sci. 10 (2016) 422–427. https://doi.org/10.1007/s11706-016-0362-8.
[57] R. Sierra-Ávila, M. Pérez-Alvarez, G. Cadenas-Pliego, V. Comparán Padilla, C. Ávila-Orta, O. Pérez Camacho, E. Jiménez-Regalado, E. Hernández-Hernández, R.M. Jiménez-Barrera, Synthesis of Copper Nanoparticles Using Mixture of Allylamine and Polyallylamine, Journal of Nanomaterials. (2015). https://doi.org/10.1155/2015/367341.
[58] Y. Yong, T. Yonezawa, M. Matsubara, H. Tsukamoto, The mechanism of alkylamine-stabilized copper fine particles towards improving the electrical conductivity of copper films at low sintering temperature, Journal of Materials Chemistry C. 3 (2015) 5890–5895. https://doi.org/10.1039/C5TC00745C.
[59] Y.-J. Kim, C.H. Ahn, M.B. Lee, M.-S. Choi, Characteristics of electrospun PVDF/SiO2 composite nanofiber membranes as polymer electrolyte, Materials Chemistry and Physics. 127 (2011) 137–142. https://doi.org/10.1016/j.matchemphys.2011.01.046.
[60] S. Janakiraman, A. Surendran, S. Ghosh, S. Anandhan, A. Venimadhav, Electroactive poly(vinylidene fluoride) fluoride separator for sodium ion battery with high coulombic efficiency, Solid State Ionics. 292 (2016) 130–135. https://doi.org/10.1016/j.ssi.2016.05.020.
[61] X. Cai, T. Lei, D. Sun, L. Lin, A critical analysis of the α, β and γ phases in poly(vinylidene fluoride) using FTIR, RSC Adv. 7 (2017) 15382–15389. https://doi.org/10.1039/C7RA01267E.

Journal Pre-proof

[62] W.A. Yee, M. Kotaki, Y. Liu, X. Lu, Morphology, polymorphism behavior and molecular orientation of electrospun poly(vinylidene fluoride) fibers, Polymer. 48 (2007) 512–521. https://doi.org/10.1016/j.polymer.2006.11.036.
[63] S.K. Karan, D. Mandal, B.B. Khatua, Self-powered flexible Fe-doped RGO/PVDF nanocomposite: an excellent material for a piezoelectric energy harvester, Nanoscale. 7 (2015) 10655–10666. https://doi.org/10.1039/C5NR02067K.
[64] M. Li, N. Stingelin, J.J. Michels, M.-J. Spijkman, K. Asadi, K. Feldman, P.W.M. Blom, D.M. de Leeuw, Ferroelectric Phase Diagram of PVDF:PMMA, Macromolecules. 45 (2012) 7477–7485. https://doi.org/10.1021/ma301460h.
[65] J. Yang, H. Chen, Z. Wang, Synthesis of sodium-potassium niobate (K, Na)NbO3 lead-free piezoelectric powders using solvothermal and hydrothermal processing, in: Proceedings of the 2010 Symposium on Piezoelectricity, Acoustic Waves and Device Applications, IEEE, Xiamen, China, 2010: pp. 249–253. https://doi.org/10.1109/SPAWDA.2010.5744314.
[66] M. Feizpour, H. Barzegar Bafrooei, R. Hayati, T. Ebadzadeh, Microwave-assisted synthesis and sintering of potassium sodium niobate lead-free piezoelectric ceramics, Ceramics International. 40 (2014) 871–877. https://doi.org/10.1016/j.ceramint.2013.06.081.
[67] C. Wang, Y. Hou, H. Ge, M. Zhu, H. Wang, H. Yan, Sol–gel synthesis and characterization of lead-free LNKN nanocrystalline powder, Journal of Crystal Growth. 310 (2008) 4635–4639. https://doi.org/10.1016/j.jcrysgro.2008.08.042.
[68] M. del C.B. López, G. Fourlaris, B. Rand, F.L. Riley, Characterization of Barium Titanate Powders: Barium Carbonate Identification, Journal of the American Ceramic Society. 82 (1999) 1777–1786. https://doi.org/10.1111/j.1151-2916.1999.tb01999.x.
[69] H. Parangusan, D. Ponnamma, M.A.A. Al-Maadeed, Stretchable Electrospun PVDF-HFP/Co-ZnO Nanofibers as Piezoelectric Nanogenerators, Scientific Reports. 8 (2018) 754. https://doi.org/10.1038/s41598-017-19082-3.
[70] J.-H. Lee, H.-J. Yoon, T.Y. Kim, M.K. Gupta, J.H. Lee, W. Seung, H. Ryu, S.-W. Kim, Micropatterned P(VDF-TrFE) Film-Based Piezoelectric Nanogenerators for Highly Sensitive Self-Powered Pressure Sensors, Advanced Functional Materials. 25 (2015) 3203–3209. https://doi.org/10.1002/adfm.201500856.
[71] S.Y. Chung, S. Kim, J.-H. Lee, K. Kim, S.-W. Kim, C.-Y. Kang, S.-J. Yoon, Y.S. Kim, All-Solution-Processed Flexible Thin Film Piezoelectric Nanogenerator, Advanced Materials. 24 (2012) 6022–6027. https://doi.org/10.1002/adma.201202708.
[72] G. Suo, Y. Yu, Z. Zhang, S. Wang, P. Zhao, J. Li, X. Wang, Piezoelectric and Triboelectric Dual Effects in Mechanical-Energy Harvesting Using BaTiO3/Polydimethylsiloxane Composite Film, ACS Appl. Mater. Interfaces. 8 (2016) 34335–34341. https://doi.org/10.1021/acsami.6b11108.
[73] G. Liu, E. Abdel-Rahman, D. Ban, Performance optimization of p-n homojunction nanowire-based piezoelectric nanogenerators through control of doping concentration, Journal of Applied Physics. 118 (2015) 094307. https://doi.org/10.1063/1.4930031.
[74] Y. Sun, J. Chen, X. Li, Y. Lu, S. Zhang, Z. Cheng, Flexible piezoelectric energy harvester/sensor with high voltage output over wide temperature range, Nano Energy. 61 (2019) 337–345. https://doi.org/10.1016/j.nanoen.2019.04.055.
[75] D. Giovanelli, E. Farella, Force Sensing Resistor and Evaluation of Technology for Wearable Body Pressure Sensing, Journal of Sensors. 2016 (2016) e9391850. https://doi.org/10.1155/2016/9391850.
[76] F. Reza, G.B. Batson, J.A. Yamamuro, J.S. Lee, Resistance Changes during Compression of Carbon Fiber Cement Composites, Journal of Materials in Civil Engineering. 15 (2003) 476–483. https://doi.org/10.1061/(ASCE)0899-1561(2003)15:5(476).

Journal Pre-proof

[77] S. Bairagi, S.W. Ali, A unique piezoelectric nanogenerator composed of melt-spun PVDF/KNN nanorod-based nanocomposite fibre, European Polymer Journal. 116 (2019) 554–561. https://doi.org/10.1016/j.eurpolymj.2019.04.043.
[78] G. Zhao, X. Zhang, X. Cui, S. Wang, Z. Liu, L. Deng, A. Qi, X. Qiao, L. Li, C. Pan, Y. Zhang, L. Li, Piezoelectric Polyacrylonitrile Nanofiber Film-Based Dual-Function Self-Powered Flexible Sensor, ACS Appl. Mater. Interfaces. 10 (2018) 15855–15863. https://doi.org/10.1021/acsami.8b02564.
[79] J. He, S. Qian, X. Niu, N. Zhang, J. Qian, X. Hou, J. Mu, W. Geng, X. Chou, Piezoelectric-enhanced triboelectric nanogenerator fabric for biomechanical energy harvesting, Nano Energy. 64 (2019) 103933. https://doi.org/10.1016/j.nanoen.2019.103933.
[80] A. Proto, M. Penhaker, S. Conforto, M. Schmid, Nanogenerators for Human Body Energy Harvesting, Trends in Biotechnology. 35 (2017) 610–624. https://doi.org/10.1016/j.tibtech.2017.04.005.
[81] A. Yu, P. Jiang, Z. Lin Wang, Nanogenerator as self-powered vibration sensor, Nano Energy. 1 (2012) 418–423. https://doi.org/10.1016/j.nanoen.2011.12.006.
[82] M.I. Friswell, S. Adhikari, Sensor shape design for piezoelectric cantilever beams to harvest vibration energy, Journal of Applied Physics. 108 (2010) 014901. https://doi.org/10.1063/1.3457330.
[83] J. Ajitsaria, S.Y. Choe, D. Shen, D.J. Kim, Modeling and analysis of a bimorph piezoelectric cantilever beam for voltage generation, Smart Mater. Struct. 16 (2007) 447–454. https://doi.org/10.1088/0964-1726/16/2/024.
[84] M. Ma, Z. Kang, Q. Liao, Q. Zhang, F. Gao, X. Zhao, Z. Zhang, Y. Zhang, Development, applications, and future directions of triboelectric nanogenerators, Nano Res. 11 (2018) 2951–2969. https://doi.org/10.1007/s12274-018-1997-9.
[85] J.P. Lee, J.W. Lee, J.M. Baik, The Progress of PVDF as a Functional Material for Triboelectric Nanogenerators and Self-Powered Sensors, Micromachines (Basel). 9 (2018). https://doi.org/10.3390/mi9100532.
[86] S. Cheon, H. Kang, H. Kim, Y. Son, J.Y. Lee, H.-J. Shin, S.-W. Kim, J.H. Cho, High-Performance Triboelectric Nanogenerators Based on Electrospun Polyvinylidene Fluoride–Silver Nanowire Composite Nanofibers, Advanced Functional Materials. 28 (2018) 1703778. https://doi.org/10.1002/adfm.201703778.
[87] X.-S. Zhang, M.-D. Han, R.-X. Wang, F.-Y. Zhu, Z.-H. Li, W. Wang, H.-X. Zhang, Frequency-Multiplication High-Output Triboelectric Nanogenerator for Sustainably Powering Biomedical Microsystems, Nano Lett. 13 (2013) 1168–1172. https://doi.org/10.1021/nl3045684.
[88] L. Gu, N. Cui, L. Cheng, Q. Xu, S. Bai, M. Yuan, W. Wu, J. Liu, Y. Zhao, F. Ma, Y. Qin, Z.L. Wang, Flexible Fiber Nanogenerator with 209 V Output Voltage Directly Powers a Light-Emitting Diode, Nano Lett. 13 (2013) 91–94. https://doi.org/10.1021/nl303539c.
[89] X. Wang, B. Yang, J. Liu, Y. Zhu, C. Yang, Q. He, A flexible triboelectric-piezoelectric hybrid nanogenerator based on P(VDF-TrFE) nanofibers and PDMS/MWCNT for wearable devices, Scientific Reports. 6 (2016) 36409. https://doi.org/10.1038/srep36409.
[90] Y. Zhu, B. Yang, J. Liu, X. Wang, L. Wang, X. Chen, C. Yang, A flexible and biocompatible triboelectric nanogenerator with tunable internal resistance for powering wearable devices, Scientific Reports. 6 (2016) 22233. https://doi.org/10.1038/srep22233.
[91] D. Yoo, E.Y. Go, D. Choi, J.-W. Lee, I. Song, J.-Y. Sim, W. Hwang, D.S. Kim, Increased Interfacial Area between Dielectric Layer and Electrode of Triboelectric Nanogenerator toward Robustness and Boosted Energy Output, Nanomaterials. 9 (2019) 71. https://doi.org/10.3390/nano9010071.
[92] Y. Yao, T. Jiang, L. Zhang, X. Chen, Z. Gao, Z.L. Wang, Charging System Optimization of Triboelectric Nanogenerator for Water Wave Energy Harvesting and Storage, ACS Appl. Mater. Interfaces. 8 (2016) 21398–21406. https://doi.org/10.1021/acsami.6b07697.

Journal Pre-proof

[93] C. Cui, X. Wang, Z. Yi, B. Yang, X. Wang, X. Chen, J. Liu, C. Yang, Flexible Single-Electrode Triboelectric Nanogenerator and Body Moving Sensor Based on Porous Na2CO3/Polydimethylsiloxane Film, ACS Appl. Mater. Interfaces. 10 (2018) 3652–3659. https://doi.org/10.1021/acsami.7b17585.
[94] K. Zhao, Y. Wang, L. Han, Y. Wang, X. Luo, Z. Zhang, Y. Yang, Nanogenerator-Based Self-Charging Energy Storage Devices, Nano-Micro Lett. 11 (2019) 19. https://doi.org/10.1007/s40820-019-0251-7.
[95] Y. Wang, Y. Yang, Z.L. Wang, Triboelectric nanogenerators as flexible power sources, Npj Flexible Electronics. 1 (2017) 1–10. https://doi.org/10.1038/s41528-017-0007-8.
[96] K. Liu, T. Ding, J. Li, Q. Chen, G. Xue, P. Yang, M. Xu, Z.L. Wang, J. Zhou, Thermal–Electric Nanogenerator Based on the Electrokinetic Effect in Porous Carbon Film, Advanced Energy Materials. 8 (2018) 1702481. https://doi.org/10.1002/aenm.201702481.
[97] R.K. Cheedarala, J.I. Song, Sand-polished Kapton film and aluminum as source of electron transfer triboelectric nanogenerator through vertical contact separation mode, International Journal of Smart and Nano Materials. 11 (2020) 38–46. https://doi.org/10.1080/19475411.2020.1727991.

Acknowledgement

Abu Musa Abdullah, Muhtasim Ul Karim Sadaf, and Farzana Tasnim acknowledge the Graduate College of the University of Texas Rio Grande Valley for the Presidential Graduate Research Assistantship. The research work was supported through US National Science Foundation PREM grant. Award # DMR 1523577.

Journal Pre-proof

Author Biography

Abu Musa Abdullah received his MS in Mechanical Engineering from the University of Texas Rio Grande Valley (UTRGV), Texas, United States in 2020. He received his B.Sc. degree in Mechanical Engineering from Bangladesh University of Engineering and Technology (BUET), Dhaka, Bangladesh in 2017. Currently, he is a Ph.D. student at the Pennsylvania State University. He also received the prestigious Presidential Graduate Research Assistantship from the Graduate College of UTRGV at 2018. His research interest includes Nanogenerator, Energy Application of Functional Nanomaterials and Renewable Energy Systems.

Journal Pre-proof

Muhtasim Ul Karim Sadaf graduated from Shahjalal University of Science and Technology, Bangladesh with a B.Sc. in Chemical Engineering and Polymer Science in Bangladesh in 2018. He is currently a graduate student in the Department of Chemistry at the University of Texas Rio Grande Valley (UTRGV). His research interests include Nanomaterials, Functional Polymers, Energy Harvesting, and Sensors. He is the recipient of the prestigious Presidential Graduate Research Assistantship, Henry Poppenhagen Endowed Scholarship, Elliot Endowed Departmental Scholarship at UTRGV.

Dr. M. Jasim Uddin obtained his Ph.D. degree (Materials Science) from University of Turin, Italy. He is currently working as an Associate Professor and Director of Photonics and Energy Research Laboratory (PERL) in the Department of Chemistry, University of Texas Rio Grande Valley. He worked at Tulane University, LA and Florida State University, FL. He is known for invention of three-dimensional solar cells,

Journal Pre-proof

and self-cleaning, antimicrobial textiles and photochromic textiles. He is recently awarded: High Scholar Research Competition Award 2016, 2018, & 2020 (UTRGV), Outstanding and Sustainable Research in Science Award 2016 (UTRGV), United Group Research Award 2016 (International), NASA Texas Space Grant Award (2016), UGC Award in 2010 (International), etc.

Journal Pre-proof

CRediT authorship contribution statement

Abu Musa Abdullah: Writing – original draft, Conceptualization, Visualization, Methodology, Validation, Investigation, Data curation, Formal Analysis. **Muhtasim Ul Karim Sadaf:** Investigation, Methodology, Visualization, Validation, Data curation, Formal analysis, Writing – review & editing. **Farzana Tasnim:** Writing – review and editing. **Horacio Vasquez:** Writing – review & editing, Visualization. **Karen Lozano:** Writing – review & editing, Visualization. **M. Jasim Uddin:** Conceptualization, Supervision, Project administration, Funding acquisition.

Journal Pre-proof

Declaration of interests

☒ The authors declare that they have no known competing financial interests or personal relationships that could have appeared to influence the work reported in this paper.

☐The authors declare the following financial interests/personal relationships which may be considered as potential competing interests:

Journal Pre-proof

Highlights

• KNN/PVDF/MWCNT based (lead free) energy film was synthesized for piezoelectric and triboelectric operation.

• The energy film was tested at variable pressure, load frequency and finger motions.

• The hybrid energy film showed high output of 54.1 V and 29.4 μA.

• The energy film can be used for lead free energy harvesting (powering small electronic devices) and multidimensional sensory operations.

Journal Pre-proof

Journal Pre-proof